

Chapter 3

Tropospheric aerosols

3.1 Introduction

The sources of tropospheric aerosols vary from gas-to-particle conversion process to mechanical processes such as wind blown dust, volcanic emissions, soot from industries, vehicle exhaust, sea spray etc. Accordingly their residence times and removal processes vary greatly. Depending on the parameter of interest the measurement techniques employed to study aerosol characteristics can vary from ground based to space borne. In this chapter a brief summary of the measurement techniques employed for determining aerosol characteristics with an emphasis on the troposphere is provided and a description of various other measurement techniques relevant to stratospheric aerosol study is deferred to Chapter 4. Measurement of aerosol characteristics can be done by ground based techniques such as Sun photometer [Volz, 1970], lidar (laser radar) [Fiocco and Grams, 1964; Jäger and Hofmann, 1991; Takamura *et al.*, 1994], particle impactors [Junge, 1963; Jaenicke and Schütz, 1978] or air borne techniques such as balloons, either with optical particle counters [Hofmann, 1993] or impactors [Bigg, 1976] and satellites [Griggs, 1983; Quenzel, 1983; Kaufman *et al.*, 1990; Kent *et al.*, 1991].

Lidar makes use of the scattered radiation from particles in the medium being probed. Based on the configuration there are two types of lidars. The monostatic lidar [Fiocco and Grams, 1964; Jäger and Hofmann, 1991] is a system in which the transmitter and the receiver are collocated, whereas in the bistatic lidar system [Herman *et al.*, 1971; Parameswaran *et al.*, 1984; Devara *et al.*, 1994] the transmitter and the receiver are

separated by a distance. While the monostatic lidar is capable of obtaining vertical profile of aerosols up to higher altitudes, the bistatic lidar can be used to study the angular distribution of the scattered intensity from a desired altitude by changing the orientation of the transmitter and the receiver, but the altitude coverage is limited to lower altitudes. The transmitter-receiver configuration determines the scattering volume. From the monostatic lidar the vertical profiles of aerosol extinction coefficients can be obtained [Parameswaran *et al.*, 1991] and in the bistatic mode the aerosol size distribution and number density can be obtained [Parameswaran *et al.*, 1984].

Sampling of particles is one of the most widely used methods to determine the physical and chemical characteristics of aerosols [Junge, 1963; Khemani *et al.*, 1982]. From the mass of aerosols collected in the various size ranges, the aerosol size distribution and the chemical composition can be determined.

Quenzel [1983] and Griggs [1983] determined the total optical depth of the medium from the scattered solar radiation intensity measurements over low albedo surfaces such as oceans. Kaufman *et al.* [1990] using the NOAA/AVHRR visible and near infrared channels determined the aerosol optical depth and particle radius from the satellite images of the surface (land and water). The aerosol optical depths were determined with an error of about 0.08-0.15 when the optical depth was in the range of 0.5-1.5. The satellite derived values were found to agree well with the Sun photometer measurements made from the ground. Determination of the aerosol optical depth using satellite data requires an a priori knowledge of the type of aerosol, aerosol phase function and single scattering albedo (ω_0). In their absence the results can only be qualitative and are useful for studying the variations in the aerosol loading [Jayaraman and Koepke, 1992]. However, the natural variability of the aerosol size distribution even at one place can create variations in the radiance measured by the satellite (for example over the Atlantic off West Africa, both maritime background aerosol and Saharan dust aerosol are present simultaneously) [Quenzel, 1983]. The next difficulty arises from the noninclusion of the multiple scattering processes in the computations of the radiation field. Especially in cases such as desert dust outbreaks the aerosol optical depths become too high to neglect the multiple scattering effect [Jayaraman and Subbaraya, 1993b]. The satellite-borne, Stratospheric Aerosol Gas Experiments (SAGE I, SAGE II) of NASA are meant for monitoring stratospheric

and tropospheric aerosols. In these measurements Sun photometers are used to determine aerosol characteristics [Kent *et al.*, 1991; Kent *et al.*, 1994]. Kent *et al.* [1994] compared the SAGE I and II data with the surface radiometer data and the results showed good agreement. Also in these experiments vertical profiles of aerosol extinction coefficients are obtained which are integrated to determine the aerosol optical depths. The presence of high-altitude clouds adversely affect the satellite borne studies on tropospheric aerosols.

Using balloonborne optical particle counters Hofmann [1993] studied tropospheric aerosol number density from 2 km above the ground, over a period of 2 decades, over Laramie, Wyoming (41°N) starting from 1971.

Sun photometry is one of the most widely used techniques for measuring aerosol properties by which the aerosol optical depths can be directly obtained, unlike other remote sensing techniques, where the data have to be analysed using complex inversion algorithms to evaluate the optical depths. The other methods require a knowledge of the type of aerosols in the medium. Also, no absolute calibration of the instrument is necessary in case of Sun photometers and comparison of results with other measurements is relatively easy, as the optical depths are directly derived. Volz sun photometry [Volz, 1970] is one of the most widely used techniques for atmospheric turbidity [Ångström, 1961; Flowers *et al.*, 1969] measurement. From the turbidity measurements attempts were also made to draw an inference on the aerosol properties [Ångström, 1961].

Direct-Sun photometry at multiple wavelengths is a useful method to characterise aerosols in the Earth's atmosphere. The technique is based on the principle of sunlight attenuation by scattering and absorption of aerosols. Generally by measuring the absolute value of ground level direct solar irradiance and comparing it to the known value of incident solar irradiance, the aerosol induced optical attenuation of the atmosphere in a narrow wavelength band is derived [Shaw, 1976]. The information on the aerosol size distribution can be obtained from the spectral variation of the extinction of light through the atmosphere, as particles of different sizes scatter light differently. An advantage of such multiwavelength Sun photometry as compared to 'point' collections of aerosols, is its relevance to the column integrated atmospheric quantities, that is, the assessment of amount of aerosol in the entire atmosphere, a quantity likely to be much more valuable to climatic investigations than surface parameters only [Shaw, 1983].

In this chapter the features of aerosol optical depths observed over Ahmedabad (23°N , 72.5°E) located in western India, an urban station with several industries, the possible aerosol type over the station is a mixture of water soluble, dust like and soot aerosols, are discussed. Soil dust, vehicle and industrial exhausts are the major sources of aerosols in Ahmedabad.

3.2 Ground based Sun-tracking photometer observations over Ahmedabad

An automatic Sun-tracking multichannel photometer was developed at the Physical Research Laboratory for aerosol measurements both at Ahmedabad (23°N , 72.5°E) as well as onboard balloons from Hyderabad (17.5°N , 78.6°E). The experimental programme was initiated to study the day to day and seasonal variations in aerosol optical depths induced due to natural and anthropogenic phenomena, for over a period of 5 years from 1991 to 1995. The observation period encompasses some of the devastating events that had strong influence on the atmosphere, namely the Gulf oil fires in early 1991 and Pinatubo volcanic eruption in mid-1991. The 'Operation Desert Storm' left about 600 naturally pressurised oil wells aflame in Kuwait in late February 1991 injecting large quantities of smoke, sulphur dioxide etc. into the atmosphere [Johnson *et al.*, 1991]. As Ahmedabad is located in the same zonal belt as Kuwait and also as the wind direction during the period is in general eastward, perturbation, if any, in the aerosol optical depth should be detectable over Ahmedabad. As the residence time of tropospheric aerosols is of the order of few months [Prospero *et al.*, 1983] measurements were repeated in 1992 during the same period in order to bring out the difference between the two data sets as a consequence of the fires. However, the Mt. Pinatubo eruption, which occurred in Philippines in June 1991 had a greater impact on the aerosol characteristics all around the globe [Stowe *et al.*, 1992] and marred the post Gulf oil fire effects. Several interesting features in aerosol optical depths and their temporal variations, revealed by the Sun-tracking photometer observations over Ahmedabad for a period of about 5 years will be discussed in this chapter.

3.2.1 Instrumentation

A six channel Sun-tracking photometer was used to measure the direct solar radiation intensities in the selected spectral bands, centered at 319, 441, 491, 736, 852 and 952 nm. However, since 1992 the 736 nm channel has been converted into 1051 nm in order to extend the spectral coverage of measurements. The data corresponding to 319 and 952 nm are used to obtain ozone and water vapour optical depths respectively, while the data corresponding to other photometers are used for aerosol studies.

Figure 3.1 shows the block diagram and photograph of the Sun-tracking photometer system. The instrument consists of a sensor assembly containing six photometers, the tracking mechanism for the zenith orientation of the photometers and a mechanical assembly consisting of a motor, gear box and slip rings to enable azimuthal tracking. Each photometer is a combination of a photodiode or a phototube and an interference filter. The field of view of the photometers is restricted to about 9° , using baffles. Hamamatsu R 765 solar blind phototube having spectral sensitivity only in the UV range has been used in the 319 nm photometer. For other wavelengths UV-100 photodiodes (EG&G) having spectral response from 200-1150 nm are used. The optical characteristics of the photometers used are given in Table 3.1. The filters are calibrated with a Beckman UV-Visible spectrophotometer (Model 3600, USA). As the performance of the filters can deteriorate with time, routine calibrations of the filters are made. The tracking of the Sun in elevation is achieved using two photodiodes mounted perpendicular to each other in the vertical direction. The freedom of rotation of the photometer assembly in the vertical direction is restricted between 0° and 90° , by means of two micro switches. The difference in the photodiode currents is amplified by means of a difference and sum amplifier. The amplified output is fed to a motor which orients the sensor assembly towards the Sun. A similar arrangement of photodiodes has been used for tracking in azimuth. Two 'view sensors' (solar cells) are mounted with an angular separation of 120° at the rear side of the tracking platform to bring the photometer assembly into the field of view of the azimuthal tracking sensors. The output currents from the photometers are converted into voltages using current to voltage convertor and the data are stored in computer through a PC add-on A/D card.

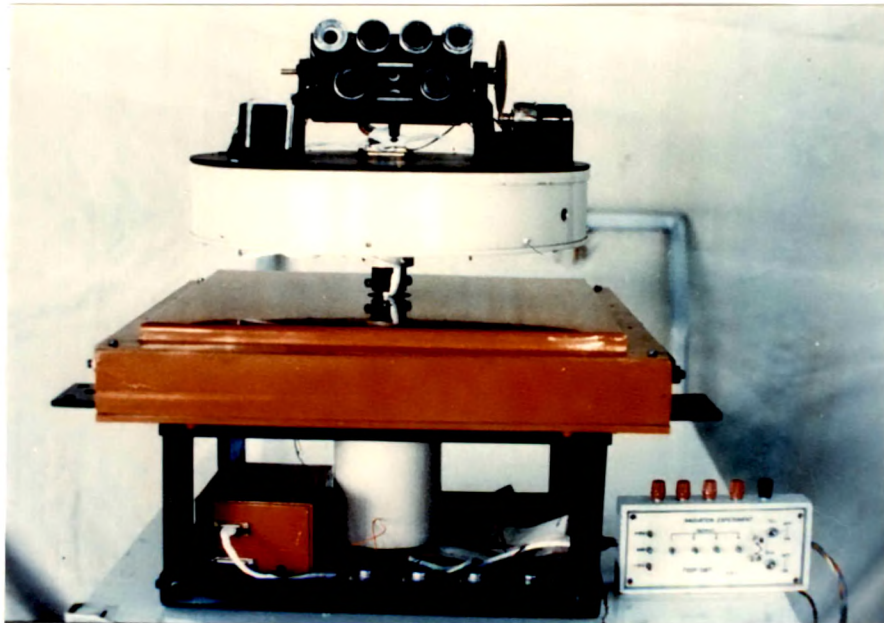
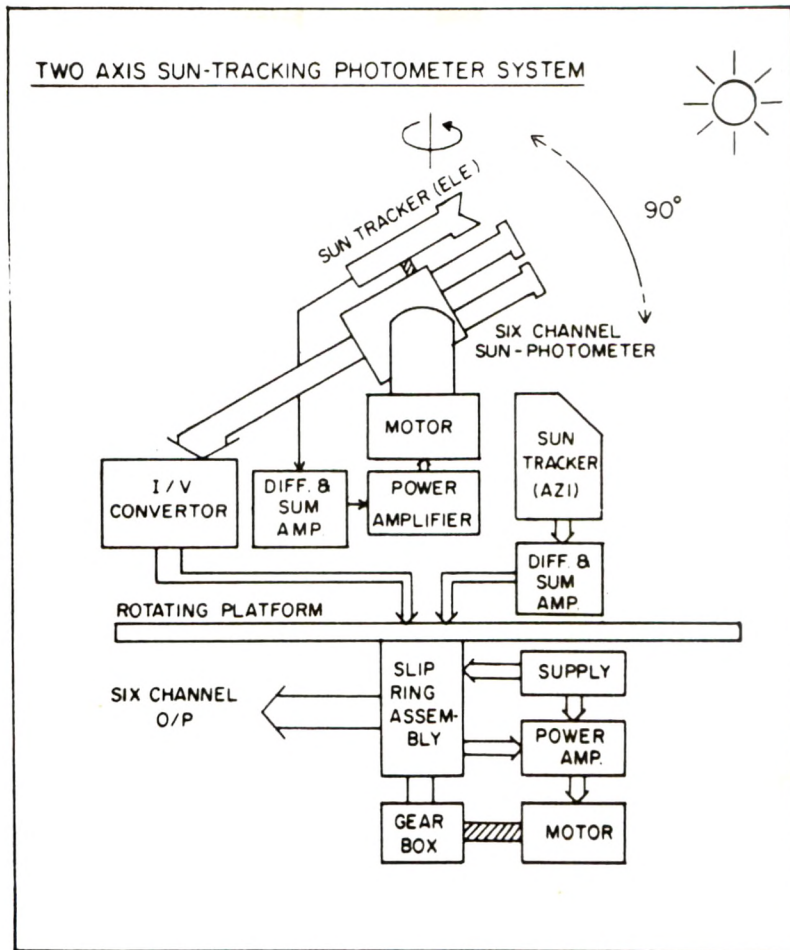


Figure 3.1: Block diagram and photograph of the six channel two-axis Sun-tracking photometer system.

Table 3.1: *Optical characteristics of the Sun-tracking photometer system.*

Channel	Center Wavelength λ_{\max} (nm)	FWHM* nm	Transmission at λ_{\max} (%)	Photodetector
1	319	15	15.4	R 765 phototube
2	441	9	33.0	UV 100 photodiode
3	491	11	34.5	-do-
4	736	17	28.0	-do-
5	852	14	21.0	-do-
6	952	20	40.0	-do-
7	1051	25	39.8	-do-

* Full Width at Half Maximum

3.2.2 Theory

The atmospheric transmission T at any wavelength λ takes the general form

$$T_i = e^{-[\sigma_i(\lambda)n_i m]} \quad (3.1)$$

for any species i under consideration, be it air, aerosol, ozone or water vapour, $\sigma_i(\lambda)$ is the corresponding absorption/scattering cross section of the species, n_i is the column density of the species and m is the air mass expressed as

$$m = \left[\frac{\sqrt{(r^2 \cos^2 \theta + 2rH + H^2)} - r \cos \theta}{H} \right] \quad (3.2)$$

where r is the radius of the Earth at the latitude of observation, H is the scale height and θ is the solar zenith angle.

However in photometry technique, measurements are taken for a wavelength band from λ_1 to λ_2 and hence an effective transmission $T_i(\text{eff})$ is to be defined to average out the variations in σ , solar flux (SF) and the detector response functions such as the filter transmission (FT) and photodiode efficiency (PE) which are all functions of λ .

$$T_i(\text{eff}) = \frac{\int_{\lambda_1}^{\lambda_2} T_i(\lambda) FT(\lambda) PE(\lambda) SF(\lambda) d\lambda}{\int_{\lambda_1}^{\lambda_2} FT(\lambda) PE(\lambda) SF(\lambda) d\lambda} \quad (3.3)$$

The transmission due to Rayleigh scattering and Rayleigh optical depths are calculated following *Penndorf* [1957]. The aerosol optical depths are calculated from the *Elterman* [1970] model. The column density of ozone over Ahmedabad was taken from the Dobson ozone data [*Angreji*, 1989] and the ozone optical depths were calculated. The water vapour optical depth is calculated from the absorptance of water vapour reported in literature [*Tanaka et al.*, 1982]. The columnar number density n of water vapour can be obtained using the relation

$$n = n_o \left(\frac{p}{760} \right) \left(\frac{273}{T} \right) \quad (3.4)$$

where n_o is Loschmidt's number = 2.687×10^{19} molecules cm^{-3} . p (= 63 torr) and T (= 296°K) are the laboratory values of pressure and temperature at which the absorptance $(1 - T)$ values are measured [*Tanaka et al.*, 1982]. From the *Water vapour atlas of India* [*Sarkar et al.*, 1982] the model humidity profiles are converted [*Hudson*, 1969] into total precipitable water content (in mm km^{-1}) or in other words, the column density of water vapour from the ground to the top of the atmosphere is obtained and used to estimate the optical depth due to water vapour absorption. The values of the solar flux at the top of the atmosphere are taken from *Nicolet* [1989] and *Thekaekara and Drummond* [1971] between 280 nm and 1100 nm. These values are multiplied by respective transmissions due to air, aerosol, ozone and water vapour in order to get the solar flux values (SF in Eqn. 3.3) at the ground.

The relative contributions of Rayleigh scattering optical depth (τ_{rs}), aerosol optical depth ($\tau_{aerosol}$), ozone optical depth (τ_{ozone}) and water vapour optical depth (τ_{water}) to the total optical depth in all the wavelength bands are shown in Figure 3.2.

3.2.3 Experiment and Data analysis

The period of measurements of the transmitted solar radiation intensities taken over Ahmedabad is listed in Table 3.2. (\checkmark indicates the months, for which the data are available for atleast 10 days and more.)

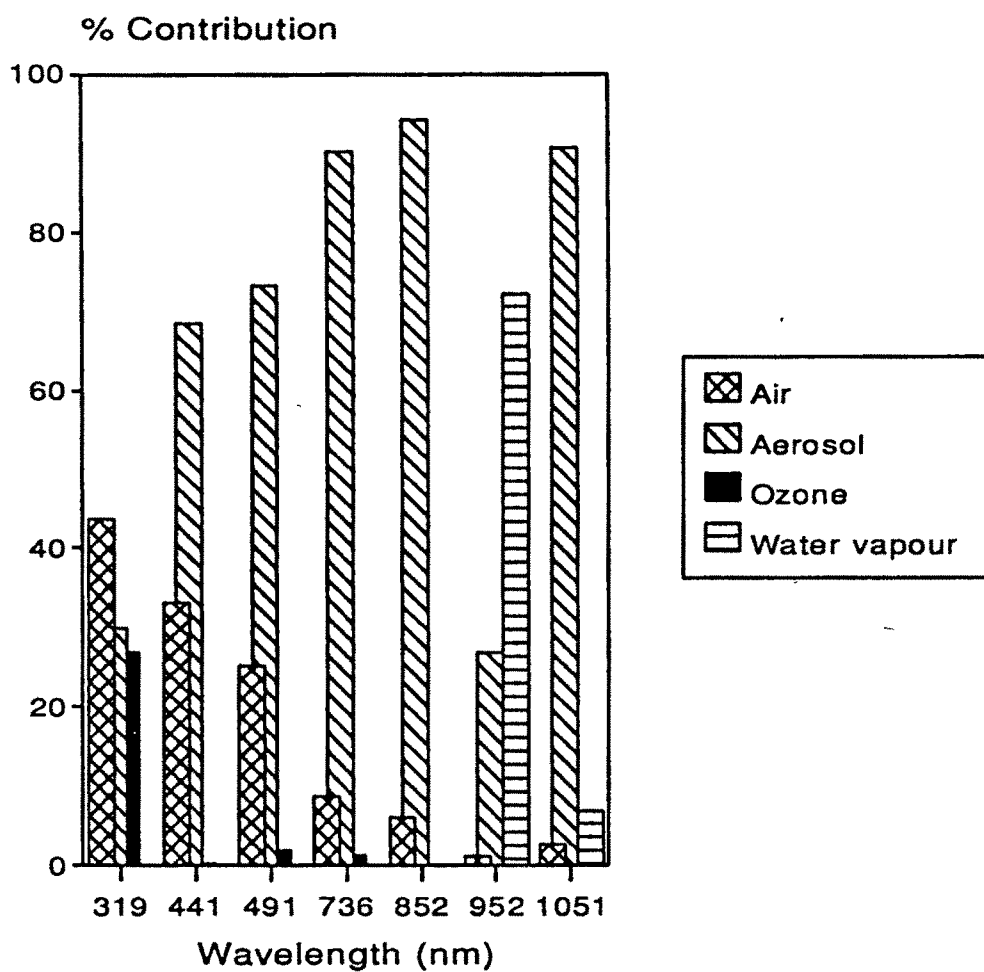


Figure 3.2: Diagram illustrating the relative contributions of air, aerosol, ozone and water vapour to the total optical depth for the respective photometers (Table 3.1) used in the present study.

Table 3.2: The period of Sun-tracking photometer observations over Ahmedabad.

Year	Months											
	J	F	M	A	M	J	J	A	S	O	N	D
1991	✓	✓	✓				Monsoon					
1992	✓	✓	✓									
1993		✓	✓	✓	✓	✓	Overcast				✓	✓
1994				✓	✓	✓				✓	✓	✓
1995	✓	✓	✓	✓	✓		sky					

The observations are taken at an interval of 10 minutes from sunrise to sunset, for various solar zenith angles. Following Beer-Lambert's law, the total integrated columnar optical depth of the atmosphere can be written as

$$\tau = \frac{-1}{m} \left[\ln \left(\frac{I}{I_0} \right) - 2 \ln \left(\frac{r_0}{r} \right) \right] \quad (3.5)$$

where I is the instantaneous solar radiation intensity measured by the photometer and I_0 is the solar radiation intensity obtained from Langley plot for zero airmass, m is the atmospheric airmass, r is the instantaneous value of the Sun-Earth distance and r_0 is the Sun-Earth distance when I_0 values are obtained. The total integrated columnar optical depth of the atmosphere

$$\tau = \tau_{rs} + \tau_{aerosol} + \tau_{ma} \quad (3.6)$$

where τ_{rs} is the Rayleigh scattering optical depth (scattering due to air molecules), $\tau_{aerosol}$ is the aerosol optical depth and τ_{ma} is the optical depth due to molecular absorptions such as ozone, water vapour or nitrogen dioxide. The aerosol optical depth $\tau_{aerosol}$ can be obtained by subtracting τ_{rs} and τ_{ma} from τ . An average air column density of 2.14×10^{25} molecules cm^{-2} derived from a series of rocket experiments [Sasi and Sengupta, 1979] is used in the estimation of τ_{rs} . The annual variation in the air column density inclusive of seasonal dispersion from January to December is not considered as it is found to be less than 2% [Sasi and Sengupta, 1986]. Differences in the total column density of air between the various reference atmospheres such as the Reference Atmosphere for Equatorial Zone [Sasi and Sengupta, 1979] and the *U. S. Standard Atmosphere* [1966] are in the range of 1% and not considered in the present work. τ_{ma} for ozone absorption is estimated using the available mean ozone column concentrations derived from Dobson measurements at Ahmedabad for over 30 years [Angreji, 1989]. The monthly mean variations in the ozone column density, which is found to be about 3 to 4% from autumn to spring is also not considered here. τ_{ma} for water vapour is estimated for each month from the monthly mean values of total column density of water vapour [Sarkar et al., 1982]. The contribution by NO_2 to the total optical depth around 440 nm where it has the maximum absorption cross section is in the range of 0.5% and less and is not considered in the present study.

The atmospheric airmass (m) is calculated from corresponding time information by

converting it to local mean time using the equation of time and solar declination angle (δ) for the day from the Astronomical Ephemeris using the equation

$$m = (\sin\delta \sin\phi + \cos\delta \cos\phi \cos H)^{-1} \quad (3.7)$$

where ϕ is the latitude of the place and H is the hour angle. For solar zenith angle greater than 60° , m is calculated taking into account the curvature of the Earth (Eqn. 3.2).

3.2.4 Determination of $I_o(\lambda)$ and Optical depth τ

$I_o(\lambda)$ values are obtained using Langley plot technique. In this technique, the natural logarithm of the photometer outputs measured for various solar zenith angles are plotted with respect to airmass. Through the experimentally observed points a least square fitted straight line is drawn and is extrapolated to meet zero airmass in the abscissa. The intercept gives $I_o(\lambda)$ of a particular photometer. Similarly, Langley plots are made to obtain $I_o(\lambda)$ for all individual photometers. The voltage $I_o(\lambda)$ obtained for zero airmass is a constant in time for a particular photometer, if the response of the instrument is constant and if the value is corrected for the mean solar distance. Since $I_o(\lambda)$ values are constant for each photometer, they can be used together with each individual photometer output I to obtain the corresponding optical depth τ using Eqn. 3.5.

To draw Langley plots observations are to be taken in a cleaner and stable atmosphere where the effects of local pollutants are minimum. These conditions are best met at high altitude mountain sites. In the present case observations are taken for a period of about one week from sunrise to sunset, at Gurushikhar (24.6°N , 72.72°E) in Mt. Abu, at a height of about 1680 metres above the mean sea level, once in a year. Mt. Abu is preferred because at Ahmedabad, industrial pollutants, vehicle smoke etc. not only pollute the atmosphere but also introduce diurnal variations in aerosol optical depth as could be seen in the Langley plot (Figure 3.3a). Drawing Langley plots and finding $I_o(\lambda)$ for individual photometer helps to calibrate the instrument once and for all. The $I_o(\lambda)$ values obtained for various photometers are given in Table 3.3. Due to technical difficulties during 1992, the photometers could not be calibrated at Gurushikhar but were calibrated in Hyderabad (17.5°N , 78.6°E), at the balloon launch station well away from the Hyderabad city.

A typical Langley plot obtained for 852 nm at Mt. Abu on 11 May 1991 is shown as

Table 3.3: $I_o(\lambda)$ values obtained at Mt. Abu using Langley plot technique.

Date	Wavelength (λ) nm					
	319	441	491	736	852	952
11 May 1991	68.84	6.97	3.23	4.07	3.04	4.40
12 May 1991	72.32	7.55	3.39	4.05	3.00	4.35
13 May 1991	79.90	7.36	3.46	4.10	3.28	4.48
14 May 1991	72.26	7.06	3.07	4.00	2.94	4.06
Mean	73.33	7.23	3.29	4.05	3.07	4.32
Sigma	4.05	0.23	0.15	0.04	0.13	0.16

an example (Figure 3.3b). In an idealised Langley plot the natural logarithm of all the observed solar radiation intensities will fall in a straight line when plotted versus airmass (m). In order to study the difference, if any, between the data collected between morning and evening hours a detailed analysis was made as suggested by *Kremser et al.* [1984], in which morning and afternoon data points are treated separately. The observations made before noon i.e. between 0700 and 1130 hrs are taken as morning data and observations made before sunset but between 1400 and 1800 hrs are taken as evening data. Langley plots are drawn for each of these data sets on all the days. The $I_o(\lambda)$ values obtained for the morning and evening data sets for each photometer are shown in Table 3.4. These values are found to compare well (within $\pm 1\sigma$) with the $I_o(\lambda)$ values obtained taking into account all the data points, indicating the stability of the atmosphere over Gurushikhar when the observations are made. The $I_o(\lambda)$ values thus obtained are used in determining the total columnar optical depths over Ahmedabad. The accuracy of the optical depths depends on the accuracy of the solar radiation intensity data with which it is measured. Due to Sun-tracking mechanism, the I values are measured with an accuracy better than 1% and as the values are digitised through an A/D card, there is no further error in retrieving I values. However, as the aerosol optical depths are obtained after correcting for the molecular contributions and ozone and water vapour optical depths, the accuracy of the derived optical depths will depend on the model values used. Also it should be noted that the $I_o(\lambda)$ values determined for each photometer have a variation around the

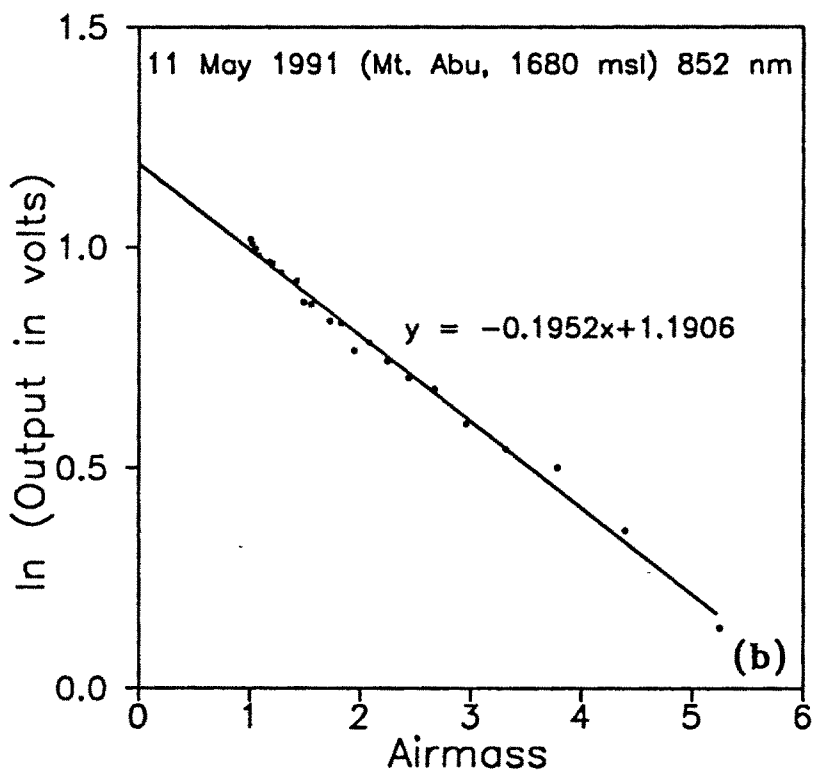
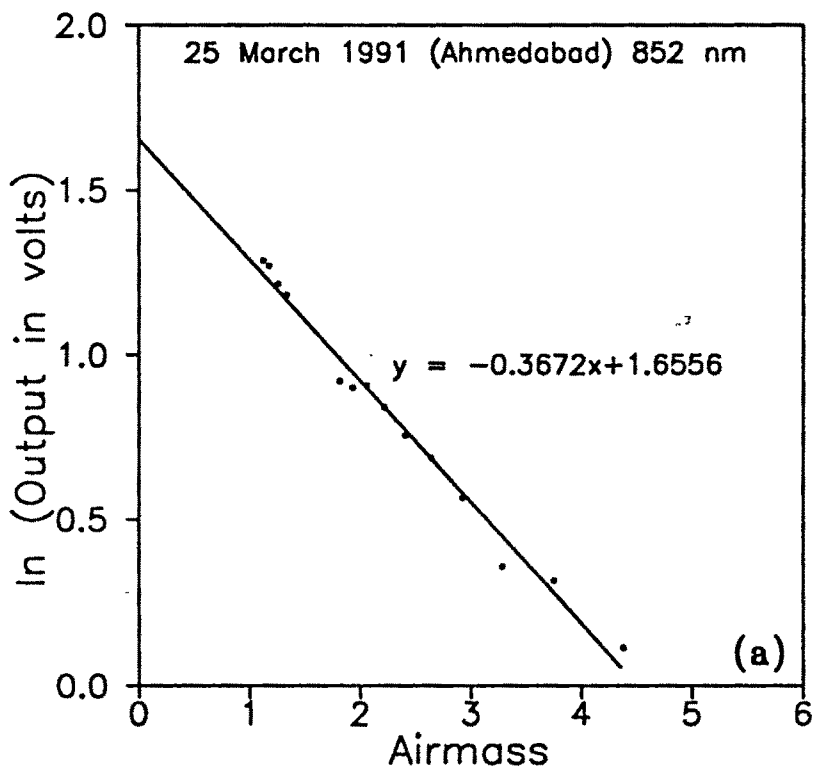


Figure 3.3: A typical Langley plot using Sun-tracking photometer data obtained at (a) Ahmedabad and (b) Mt. Abu (1680 m above msl).



Table 3.4: Comparison of $I_o(\lambda)$ values obtained using Langley plot technique for morning and evening and the $I_o(\lambda)$ values used in calculation.

Date	Session	Wavelength (λ) nm					
		319	441	491	736	852	952
11 May 1991	Morning		6.34	3.09	3.97	2.95	4.19
	Evening		7.13	3.38	4.36	3.18	4.49
12 May 1991	Morning		6.50	3.56	4.08	2.79	4.82
	Evening		7.96	3.47	4.36	3.17	4.25
13 May 1991	Morning		6.22	3.31	4.38	3.18	3.85
	Evening	72.38	7.51	3.48	4.34	3.28	4.26
14 May 1991	Morning		5.74	2.97	3.86	2.90	3.79
	Evening	66.39	6.17	3.00	3.78	2.90	3.16
	Mean	69.38	6.70	3.28	4.14	3.04	4.10
	Sigma	2.99	0.71	0.22	0.23	0.17	0.47
$I_o(\lambda)$ values used		73.33	7.23	3.29	4.05	3.07	4.32

mean value as shown in Table 3.3. This uncertainty in $I_o(\lambda)$ can introduce an error as high as 70% in the derived optical depth values, depending on the Sun position (solar zenith angle variation) as well as the turbidity on a particular day. It is noted that for high optical depth values (as it is encountered over Ahmedabad in most of the cases) the uncertainty in the optical depths will be less (less than 30%).

Since the same instrument was flown later on balloon in October 1991, some changes had to be done to accommodate one more gain level and the electronics was also changed and hence the difference in I_o values between 1991 and the rest of the years. Though the differences in $I_o(\lambda)$ values are of the order of $\pm 10\%$ during 1992 to 1995 (Table 3.5), between two successive years, the aerosol optical depths are calculated using the $I_o(\lambda)$

Table 3.5: $I_o(\lambda)$ values obtained during 1992 to 1995 and corrected for the Sun - Earth distance.

Year	Wavelength (λ) nm					
	319	441	491	852	952	1051
1992	1.69	2.42	2.01	2.15	1.00	2.39
1993	1.57	2.59	2.15	2.12	0.98	2.30
1994	1.54	2.60	1.97	2.03	0.93	2.20
1995	1.73	2.76	2.27	1.87	0.98	2.50

values as appropriate for each observation period.

The aerosol optical depths obtained are further analysed using Ångström's power law

$$\tau_{\text{aerosol}} = \beta \lambda^{-\alpha} \quad (3.8)$$

where β and α are Ångström parameters commonly used to describe the columnar distribution of aerosols. The wavelength exponent α describes the size distribution parameter of aerosols. Higher the α value smaller the aerosol particle size and vice versa. β is directly proportional to the amount of aerosol particles along the Sun path [Ångström, 1961].

Though observations are taken at Ahmedabad throughout the day, aerosol optical depths obtained between 1100 and 1200 hrs only are used to derive the wavelength exponent and their day to day variations are studied. A fixed time was chosen in preference to the daily average since the aerosol optical depths normally show a diurnal variation.

3.3 Results and Discussion

3.3.1 Diurnal, day to day and monthly variations in aerosol optical depths over Ahmedabad

About 40 observations of solar radiation intensities are made each day over Ahmedabad and aerosol optical depths are derived using the procedure outlined above. On most of the

occasions the obtained aerosol optical depths are found to show diurnal type variation. In Figure 3.4 the diurnal variations of aerosol optical depths obtained on three typical days in the months of January, February and March, for the 491 nm channel, during the year 1991 are shown as an example.

As discussed earlier no separate attempts have been made to obtain I_0 on individual days, instead the I_0 values derived for individual channels from Mt. Abu/Hyderabad are used. Hence the observed diurnal type variations could be due to the uncertainty in the derived I_0 values. However, actual diurnal variation in aerosol optical depths in an urban situation can also not be ruled out as discussed by *Shaw* [1976], in which case the apparent zero airmass intercept I_0 can be lower than the true I_0 , with a resultant decrease in τ . It has been argued that in an urban situation, τ can increase in morning hours, when urban pollutants are emitted under a capping radiative inversion. However after noon hours, under solar heating, the inversion breaks down and convection currents which set in can ventilate the trapped pollutants out of the city limits and hence a reduction in the total columnar aerosol optical depth. This feature is seen at all wavelengths and on almost all days [*Ramachandran et al.*, 1994a]. The same feature was seen by *Pinker et al.* [1994] during the 'Harmattan' season in sub-Saharan Africa. This season brings in Saharan dry and dust laden air. But sometimes, the aerosol optical depths were found to be quite stable with little diurnal variability. The diurnal variability was explained on the basis of diurnal wind effects which could have brought in more dust laden air. The optical depths are high, of the order of 0.9-1.6 at 500 nm due to very dense dust. Over Vienna and Santiago de Chile the daily patterns of aerosol optical depths are different [*Horvath*, 1993]. In Vienna the aerosol optical depth peaks at 0800 and 1800 hrs very close to the peak traffic hours, indicating the influence of the vehicular traffic on the light absorption of aerosol. But in Santiago de Chile the aerosol optical depth peaks at around 0830 hrs and then decreases, the decrease has been attributed to the continuous increase in the height of the mixing layer during the daytime. The measurements of aerosol optical depths by *Weller and Leiterer* [1988] using a Sun-calibrated spectrophotometer off the Crimea Black Sea coast also show diurnal variations. But the measurements over Tsumeb (18°E, 19°S, a semiarid region in Namibia) revealed that the aerosol optical depths are quite stable during the day [*Kremser et al.*, 1984].

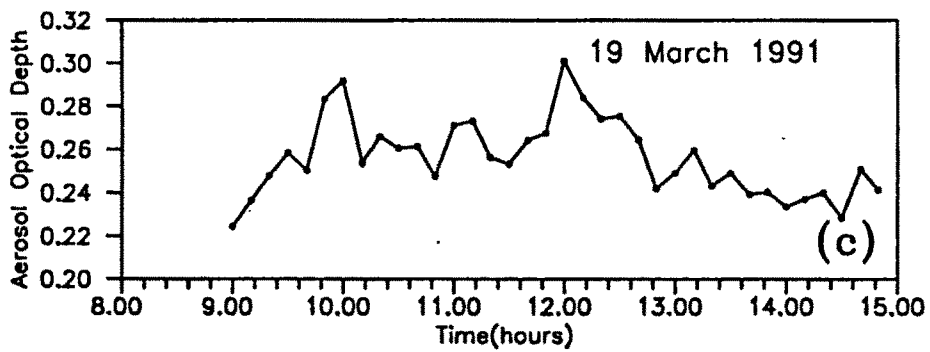
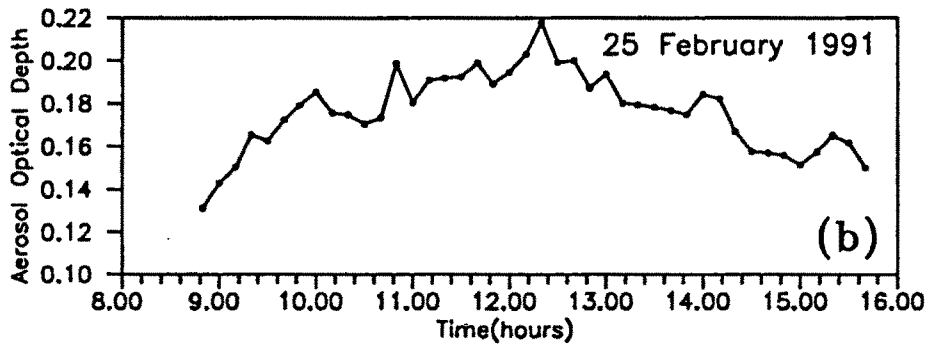
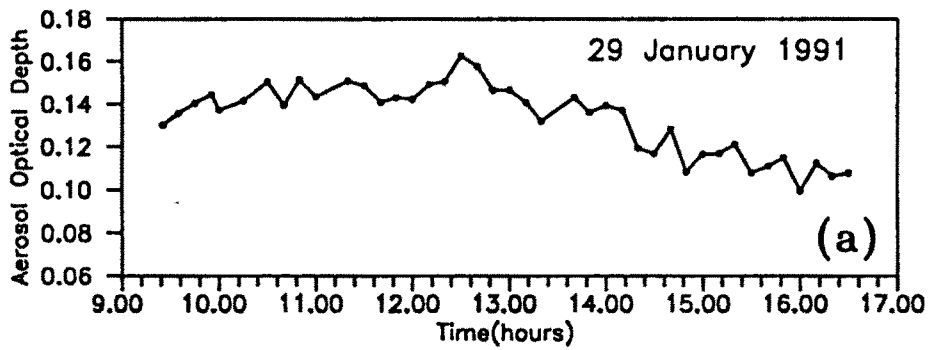


Figure 3.4: Diurnal variation of aerosol optical depths obtained over Ahmedabad for 491 nm channel during 1991.

The aerosol optical depths also exhibit large day to day variations as shown in Figure 3.5. (As an example, to depict the daily variations in aerosol optical depths, data obtained during 1991 and 1992 are shown.) As 319 nm and 952 nm photometer data are used for ozone optical depth and water vapour optical depth calculations, they are not included in the figure, but are shown separately. The day to day variations in optical depths are found to be associated with changes in meteorological parameters such as temperature and surface wind speed and direction. The aerosol optical depth values are also found to increase in general from January to March. As an example the 491 nm data, are shown in Figure 3.6 where the monthly mean values of the aerosol optical depth are plotted for the January to March 1991 period. This feature is seen at all the wavelengths in 1991 as well as in subsequent years' data sets. Similar feature has been reported earlier [Flowers *et al.*, 1969; Krishna Moorthy *et al.*, 1993] for other locations. The increase in optical depth is in general due to the increased surface temperature and low soil moisture content which can induce injection of more soil derived particles into the atmosphere. Photochemical activities [Pueschel *et al.*, 1972] can also play a role in producing aerosols *in situ* at lower tropospheric altitudes, but their seasonal dependence, if any, is not well known. The monthly mean aerosol optical depths obtained at 441 nm for the year 1993 are plotted in Figure 3.7.

By and large the aerosol optical depths are found to increase from January to May, all the years and after the monsoon rains, during which the particles get rainwashed, the aerosol optical depths are found to decrease during October to December period. As the aerosols over Ahmedabad are mainly wind blown dust particles, mechanically generated by the action of wind on dry land, the aerosol optical depths are found to increase from winter (December, January, February) to summer (April, May, June), by a factor of 4. The increase is attributed to the increased convective activity due to the increased surface heating in summer, which reduces the soil moisture content, thus inducing more soil derived particles into the atmosphere. Also, as these aerosols are large, about 1 μm , they are confined to the lower troposphere and are not lifted to higher altitudes, but are removed by sedimentation and monsoon rains, during the June-September period. Though these features in general are seen in all the years, 1993 data are shown for illustration. Similar features have been observed by Krishna Moorthy *et al.* [1993]

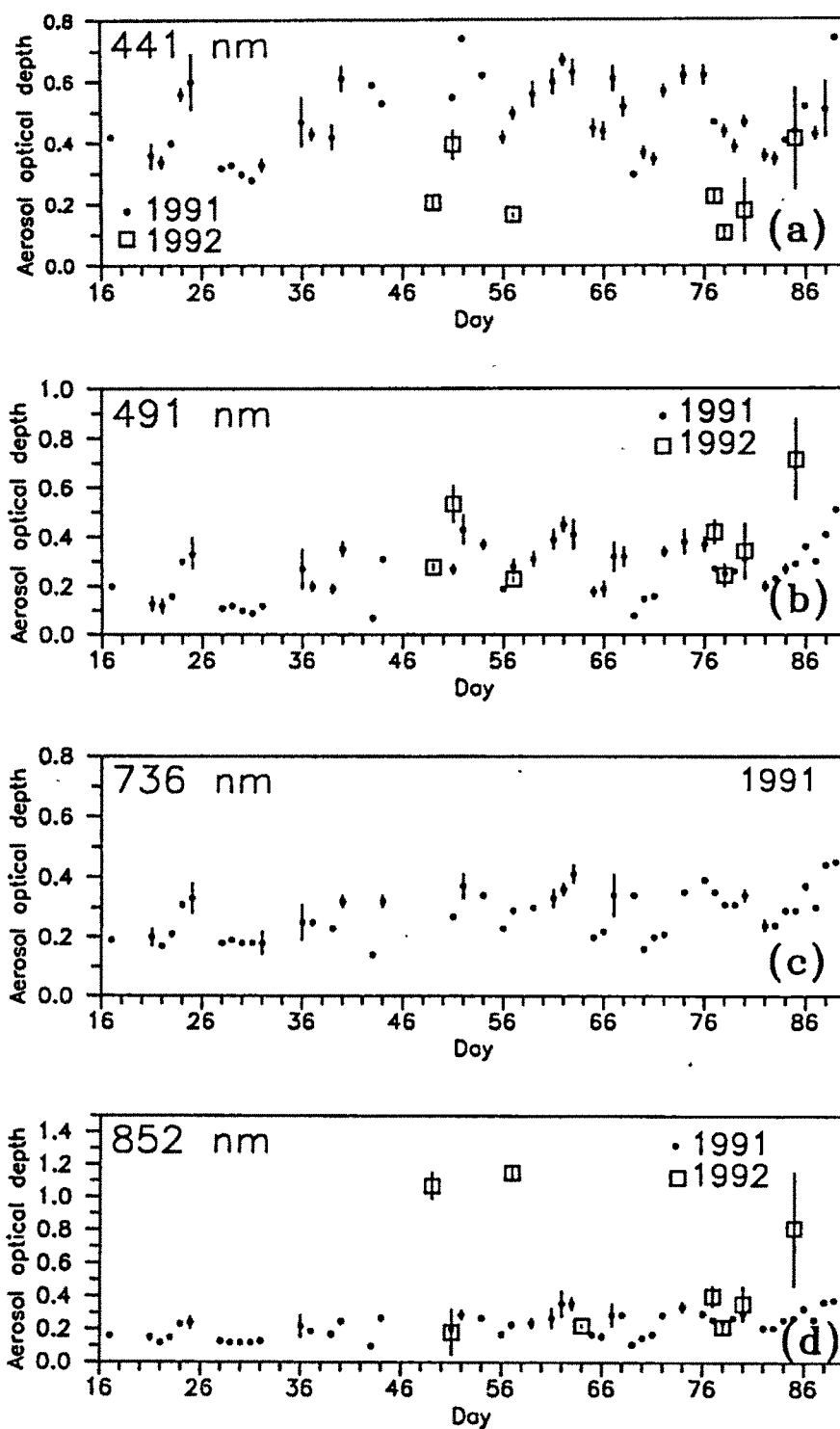


Figure 3.5: Day to day variation of aerosol optical depths for 441, 491, 736 and 852 nm. Mean of the data obtained during 1100 to 1200 hrs are shown. Vertical error bars represent two standard deviations ($\pm 1\sigma$) of the mean.

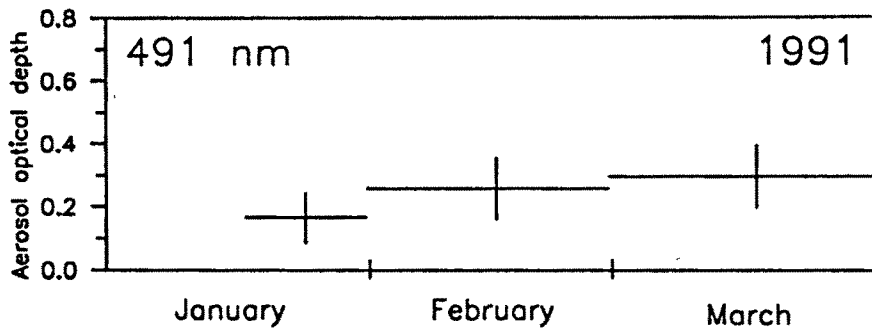


Figure 3.6: Variation of the monthly mean aerosol optical depth for the 491 nm channel. Vertical bars represent $\pm 1\sigma$ of the mean.

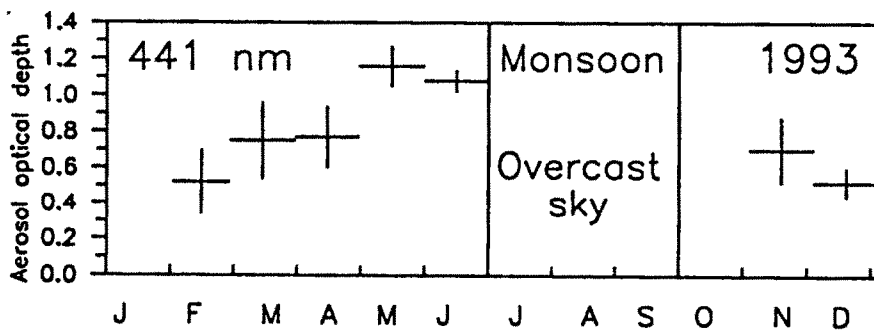


Figure 3.7: Variation of the monthly mean aerosol optical depths for the 441 nm channel for the year 1993. Vertical bars represent $\pm 1\sigma$ of the mean.

using multiwavelength radiometers at different locations in India, representing different geographical areas, comprising of coastal stations, arid regions and urban stations.

3.3.2 Spectral dependence of aerosol optical depth

The spectral dependence of the aerosol optical depth is mainly governed by the aerosol columnar size distribution. Using matrix inversion methods, multiwavelength radiometer measurements of τ_{aerosol} could be analysed to find the total columnar size distributions, when the spectral dependence is nonmonotonic. *King et al.* [1978] developed a method for such inversion. Using multiwavelength radiometer data, they deduced the columnar size distributions. The distributions are classified into three types. A monotonically decreasing $\tau_{\text{aerosol}} - \lambda$ variation gives an inverse power law size distribution as

$$\frac{dn(r)}{d(\log r)} = cr^{-\nu} \quad (3.9)$$

where $n(r)$ is the total number density of aerosols between r and $r+dr$, r is the radius of aerosol particle, c is a constant and ν is the power law exponent. The value of ν is the slope of the fitted straight line. This distribution is referred to as Type 1 (Junge distribution). Type 2 size distribution is a monomodal type distribution with a distinct maximum in the number density at a particular value of r . Type 2 results from a $\tau_{\text{aerosol}} - \lambda$ variation with a negative curvature. The size where $dn(r)/d(\log r)$ peaks depends upon the maximum in the $\tau_{\text{aerosol}} - \lambda$ variation. Type 3 results from a $\tau_{\text{aerosol}} - \lambda$ variation with a positive curvature. This distribution resembles a bimodal type distribution with 2 peaks, one in the smaller radius range and the other in the larger radius range [*Krishna Moorthy et al.*, 1991].

As the present observations of aerosol optical depths are available only at four wavelengths, it is not possible to use a detailed inversion method which requires observations at more wavelengths (six or more), to obtain quantitatively reliable size distributions. However, the nature of aerosol size distributions can be inferred as follows: the spectral dependence of τ_{aerosol} plots showed a positive curvature in 1991 indicating bimodal type size distribution, with one radius peaking below $0.5 \mu\text{m}$ and the other at $0.75 \mu\text{m}$. But in 1992 the spectral dependence showed a negative curvature indicating a monomodal type distribution, peaking at a radius of $0.5 \mu\text{m}$. *Asano et al.* [1993] using ground based

Sun photometry have also shown that at Tsukuba (36.1°N, 140.1°E) during 1991 the volume size spectra exhibit a bimodal feature with enhancements at smaller and larger radii above 0.5 μm which they attributed to tropospheric aerosols and the 1992 data exhibit a monomodal size distribution similar to the present results with the maximum radius at around 0.6 μm compared to 0.5 μm in the present case. Considering the aerosol production mechanisms, particles with sizes $\leq 0.5 \mu\text{m}$ are produced by a combination of nucleation from the gas phase and coagulation processes, whereas particles with sizes $\geq 1 \mu\text{m}$ are mainly the result of mechanical and wind stresses at the Earth's surface [King *et al.*, 1978]. The urban aerosol particles are in the size range from 0.1 μm to 1 μm (wind blown dust). A combination of the different production mechanisms may result in a bimodal distribution because of the distinct nature of these sources. A monomodal distribution would result when a strong source dominates over other sources. From the above discussion, it is seen that in 1991 (bimodal), there are two dominating sources, of which one could be of the smoke particles derived from the Gulf oil fires and the other could be the local wind derived mineral particles. In the case of 1992 data, the effect of post-volcanic aerosols due to Mt. Pinatubo can not be ruled out as also shown by Asano *et al.* [1993].

But the spectral variation curves obtained during February 1993 show a monomodal distribution, March 1993 data shows a bimodal distribution, while during summer months of May and June two peaks are seen, one at 0.44 μm and the other at 1.05 μm , which indicates the presence of larger particles, during summer. In the absence of a continuous data set, over this region, these results can only be taken as qualitative. Similar features of spectral variations have been observed by Weller and Leiterer [1988] and Krishna Moorthy *et al.* [1993]. The 1994 data in all the months, exhibit a peak at 0.5 μm and the aerosol optical depth remains almost the same for the other wavelengths. The aerosol optical depths are found to exhibit similar variations in 1995 also.

3.3.3 Variations in wavelength exponent α

The aerosol optical depth values when plotted against wavelength on a log-log scale, then the slope of the fitted line yields the wavelength exponent (α). It should be noted that while the 1991 τ_{aerosol} values could be fitted with λ with goodness of fit greater than

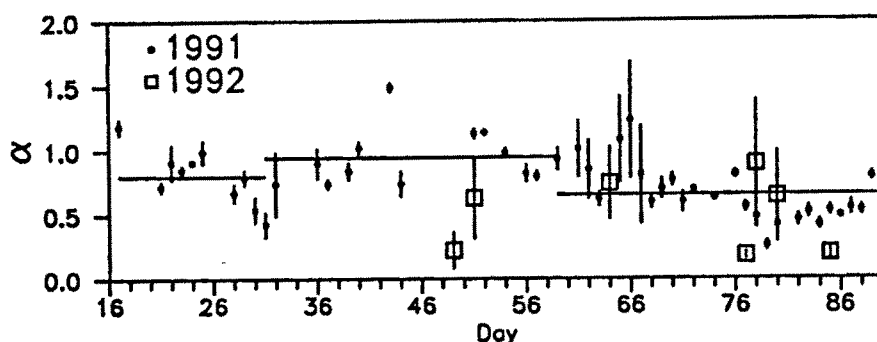


Figure 3.8: Variation in wavelength exponent, α from January to March in 1991 and 1992. The horizontal bars represent the monthly mean α values for the January-March, 1991 period.

0.9, no simple function is found between τ_{aerosol} and λ in the 1992 data on most of the occasions. This holds good for the 1993, 1994 and 1995 data sets also. The α values in the case of 1992 are limited to only a few occasions. The wavelength exponent α when plotted with respect to days (Figure 3.8) shows an oscillating behaviour. The monthly mean α values of 1991 data are also shown.

The mean α value for February is found to be higher than that of January but decreases in March. While for Rayleigh scattering $\alpha = 4$, for aerosol or Mie scattering α decreases with the increasing size of particles. Low α values in March indicate the predominance of bigger particles which can be attributed to wind blown dust. Dust storm activity also shows an increase during this period in the arid and semiarid regions of Gujarat and Rajasthan.

3.3.4 Variations in ozone optical depth

The daily mean ozone optical depth for the January to March 1991 period is plotted in Figure 3.9a. The vertical bars represent two standard deviations ($\pm 1\sigma$). The ozone optical depth values are then converted into ozone column density values in Dobson units and compared (Figure 3.9b) with the ozone column density values measured using the Dobson spectrophotometer available in PRL. The photometer derived values are consis-

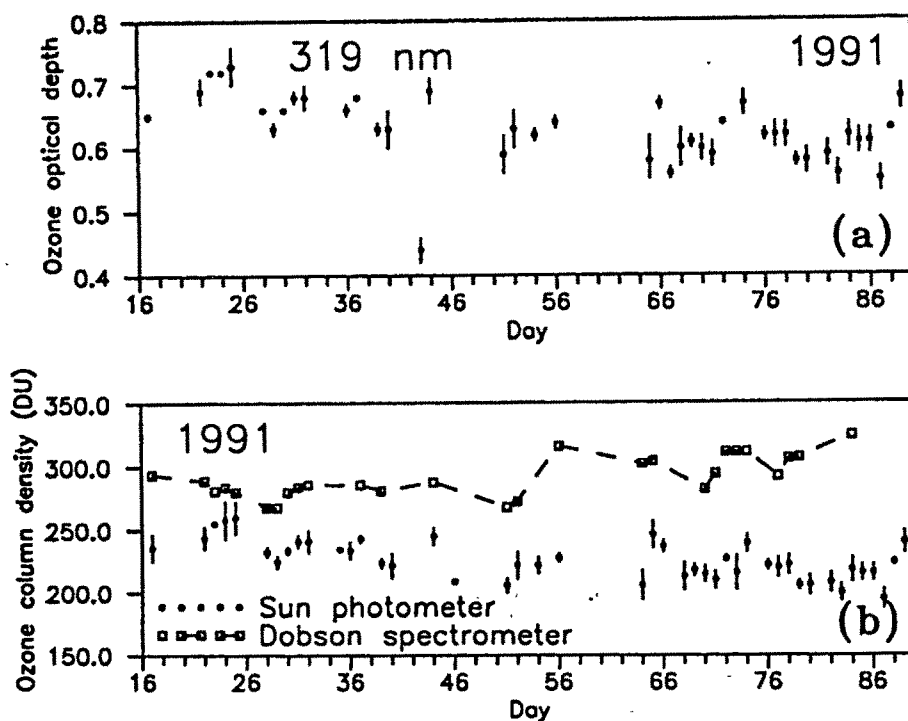


Figure 3.9: (a) Variations in ozone optical depth at 319 nm. Mean of the data obtained during 1100 to 1200 hrs are shown. Vertical bars represent $\pm 1\sigma$ of the mean. (b) Total column density of ozone, expressed in Dobson Units (DU) obtained during January-March, 1991 from Sun photometer measurements are compared with that of Dobson spectrophotometer measurements, both made at Ahmedabad. Mean of the data obtained during 1100 to 1200 hrs are shown. Vertical bars represent $\pm 1\sigma$ of the mean.

tently lower than the Dobson spectrophotometer values. The difference varies from day to day and is generally between 40-50 Dobson units, but occasionally as large as 80 Dobson units.

Similar findings are reported earlier [Shaw, 1979; Acharya et al., 1985] with observations made in the Chappuis band of ozone absorption, in which the ozone values are consistently lower than the Dobson spectrophotometer values by about 40 Dobson units. Shaw [1979] discusses sources of error in the ozone measurements done in ultraviolet region due to changes in the solar output. While discussing the systematic errors Shaw [1979] reports that errors could arise due to the wrong assumption of atmospheric airmass or

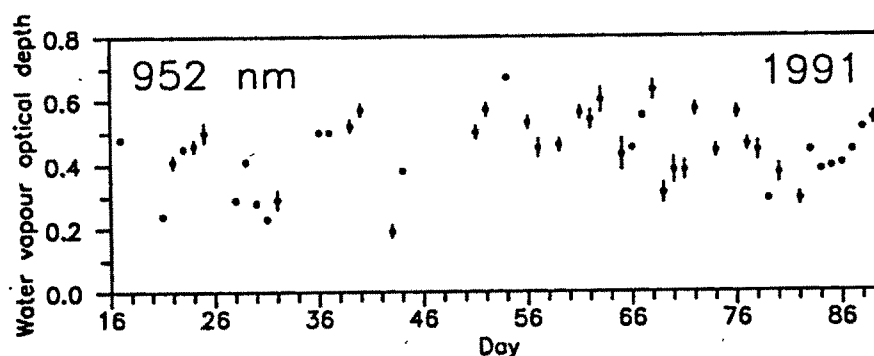


Figure 3.10: Variations in water vapour optical depth (at 952 nm) obtained during January-March, 1991. Mean of the data obtained during 1100 to 1200 hrs are shown. Vertical bars represent $\pm 1\sigma$ of the mean.

from diurnal variations of aerosol optical depth. Also he concludes that if ozone is to be measured using the Chappuis band method to anywhere near the accuracy obtainable with a Dobson spectrometer, the experiments would have to be made from high altitude locations with low turbidity. Computations show that the percentage contributions of ozone absorption is about 27% and the aerosol extinction is about 30% to the total optical depth at 319 nm wavelength region, which are comparable. Hence, reliable estimation of ozone column amounts from UV extinction measurements is possible only in locations of low turbidity, unlike Ahmedabad.

3.3.5 Variations in aerosol optical depth with relative humidity and temperature

To investigate the effect of meteorological parameters on the aerosol optical depths, the optical depths are studied with respect to relative humidity and temperature. Figure 3.10 shows the water vapour optical depths obtained at 952 nm during 1991.

Water vapour in the atmosphere affects the aerosol, by aiding it to grow bigger or shrink in size. The growth of aerosol particle results in a change in the size distribution of the aerosol particles and changes the overall refractive index of the aerosol particle, thereby affecting the optical depth by altering the scattering characteristics [Hänel, 1976].

At a coastal station where maritime aerosols are predominant, the aerosol optical depth increases as the relative humidity increases [Krishna Moorthy et al., 1993] as shown by the Shettle and Fenn [1979] model. But in Ahmedabad, the aerosols are of urban type and mineral dust forms the prime component, which are nonhygroscopic. The scatter plot (Figure 3.11a) of the daily mean (1100 to 1200 hrs data) of the aerosol optical depth with the corresponding relative humidity does not show any positive increase in the optical depth with relative humidity as it has been the case with maritime aerosols, but a general decreasing trend is seen with increasing humidity probably due to the fact that a rise in humidity increases the soil moisture content which inhibits the production of soil derived particles. Similarly the aerosol optical depths are found to increase as the day's maximum temperature increases (Figure 3.11b), which further proves the above conclusion that the rise in temperature promotes further input of soil derived particles into the atmosphere. These results are seen in all the photometers, but the results of 491 nm photometer for the year 1991 are shown here as an example. Similar results are obtained for the 1993, 1994 and 1995 years data. The trend indicates that for an increase of about 10°C in the surface temperature, the aerosol optical depth increases by about 0.2, whereas for an increase of 10% in relative humidity, the aerosol optical depth decreases by less than 0.01, showing no significant dependence.

The Ångström wavelength exponent (α) values obtained in 1991 were analysed for variations in relative humidity and are shown in Figure 3.12. As in Ahmedabad, aerosols are of urban type and mineral dust is the prime component we see a very feeble dependence of α on the varying relative humidity. As shown in Chapter 2 for Urban and Average continental models, α values almost remained the same throughout the relative humidity range of 0% to 80% and variations could be found beyond that range.

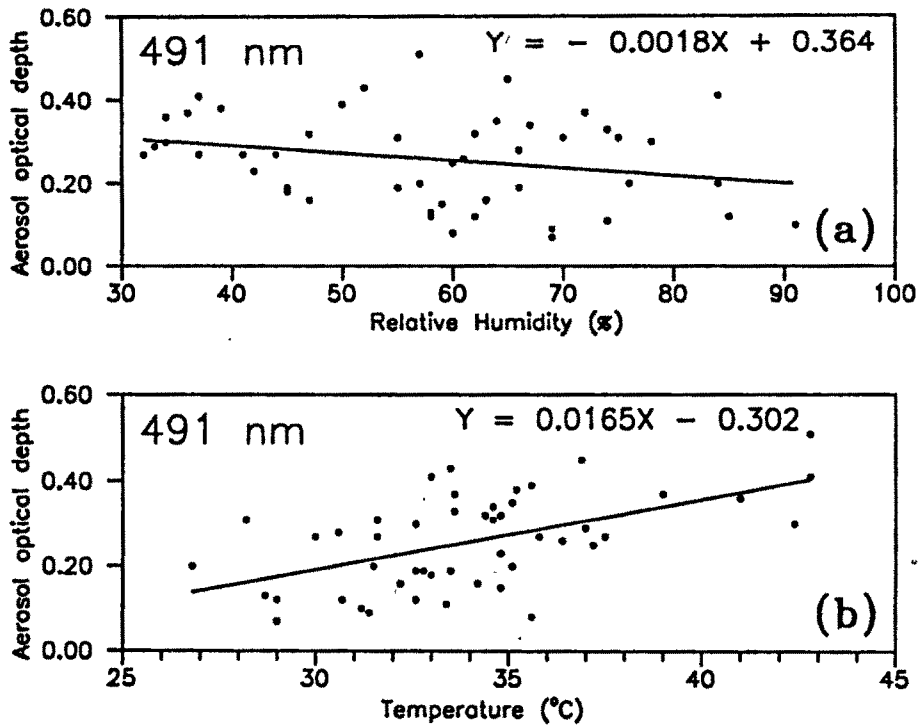


Figure 3.11: Dependence of aerosol optical depth (at 491 nm) on (a) relative humidity and (b) on the day's maximum temperature, during 1991. (Relative humidity and temperature data source: India Meteorological Department.)

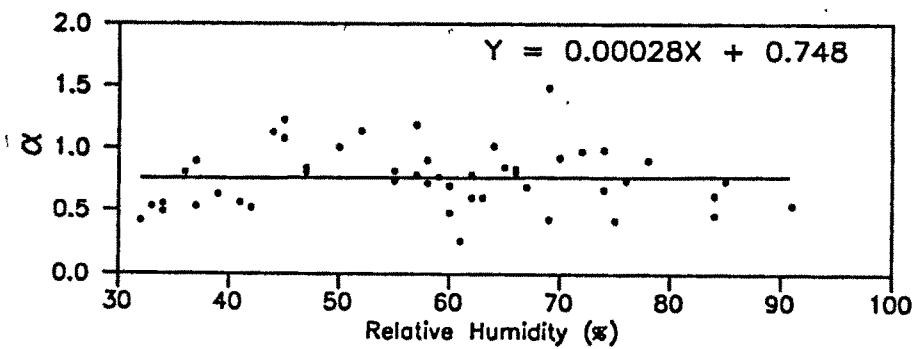


Figure 3.12: Wavelength exponent, α obtained during 1991 is plotted against measured relative humidity values. No significant dependence between the two parameters is found over Ahmedabad.